J. Phys.: Condens. Matter **21** (2009) 164209 (9pp) doi:10.1088/0953-8984/21/16/164209

Multiband superconductivity in Pb, H under pressure and CaBeSi from *ab initio* calculations

C Bersier[1,2], A Floris[1,2], P Cudazzo[3], G Profeta[3], A Sanna[1,2,4], F Bernardini[4], M Monni[4], S Pittalis[1,2], S Sharma[1,2], H Glawe[1,2], A Continenza[3], S Massidda[4] and E K U Gross[1,2]

[1] Institut für Theoretische Physik, Freie Universität Berlin, Arnimallee 14, D-14195 Berlin, Germany
[2] European Theoretical Spectroscopy Facility–ETSF, Spain
[3] CNISM—Dipartimento di Fisica, Università degli Studi dell'Aquila, Via Vetoio 10, I-67010 Coppito (L'Aquila), Italy
[4] SLACS-INFM/CNR, and Dipartimento di Scienze Fisiche, Università degli Studi di Cagliari, I-09042 Monserrato (CA), Italy

Received 22 January 2009
Published 31 March 2009
Online at stacks.iop.org/JPhysCM/21/164209

Abstract
Superconductivity in Pb, H under extreme pressure and CaBeSi, in the framework of the density functional theory for superconductors, is discussed. A detailed analysis on how the electron–phonon and electron–electron interactions combine together to determine the superconducting gap and critical temperature of these systems is presented. Pb, H under pressure and CaBeSi are multigap superconductors. We will address the question under which conditions does a system exhibits this phenomenon. The presented results contribute to the understanding of multiband and anisotropic superconductivity, which has received a lot of attention since the discovery of MgB_2, and show how it is possible to describe the superconducting properties of real materials on a fully *ab initio* basis.

(Some figures in this article are in colour only in the electronic version)

1. Introduction

The possibility of multiband superconductivity was proposed [1] a few years after the formulation of BCS theory and was later experimentally observed [2–4]. In this regard, the details of the band (n) and $\mathbf{k}$ dependence of the superconducting (SC) gap were analyzed for many materials like Pb [5–7] and Sn [8]. The recent discovery of two-gap superconductivity in MgB_2 has renewed interest in this phenomenon. Theoretical and experimental investigations have emphasized the importance of multiple gaps in the enhancement of the critical temperature T_c. Theoretical estimates have shown that including the information about the σ, π band dependence of the electron–phonon (e–ph) interaction in MgB_2 greatly enhances the calculated T_c and improves the agreement with experiment, as compared to an averaged, single-band, calculation [9–12]. Therefore of crucial importance is the question: when does the presence of multiple gaps occur and how does it affect T_c? In this context, it is very interesting to investigate the different materials showing this peculiarity.

Recently, a novel approach to superconductivity, based on density functional theory (SCDFT) [13, 14], has been able to describe, in a completely parameter-free fashion, the superconducting properties of several materials, ranging from the weak and intermediate to the strong coupling regime [12–14] and from ambient to high pressure conditions [15, 16]. Unlike in the Eliashberg theory, in SCDFT the Coulomb interaction is treated on the same footing as the electron–phonon interaction. This is crucial for determining T_c accurately.

In this work, we solve the SCDFT gap equation in a fully $(n, \mathbf{k})$-resolved formalism and calculate from first-principles the SC properties of Pb, H under pressure and CaBeSi. Within this approach all the features of the SC gap emerge naturally, without any *a priori* material-specific physical model or adjustable parameters. Our results confirm

the experimental finding that Pb is a two-band superconductor. The calculated gaps, their overall anisotropy and the T_c result in good agreement with experiments reported in [17, 18]. A T_c enhancement of ≈8% can be directly related to the presence of multiple gaps [19].

The SCDFT, with its truly *ab initio* character, allows us not only to provide a better understanding of experimental facts, but also, and more importantly, to predict the superconducting nature of systems which are not yet experimentally realized. One prime example among those is H under extreme pressure. The possibility of high temperature superconductivity in metallic hydrogen was suggested in 1968 by Ashcroft [20]. Since then it has represented one of the most fascinating and intriguing topics involving fundamental issues ranging from the limits of phonon mediation in the superconducting phenomenon to implications in astrophysics [21]. In the following we show that SCDFT predicts electron–phonon-mediated superconductivity in H, with T_c values up to 242 K at 450 GPa.

Another system for which SCDFT predicts multigap SC is CaBeSi [22], a material isostructurally isoelectronic to MgB_2. Despite the many similarities with MgB_2, according to our calculations CaBeSi has a very low critical temperature ($T_c \approx$ 0.4 K), consistent with experiment [23]. However, CaBeSi exhibits a complex gap structure, with three distinct gaps at the Fermi level.

This paper is organized as follows: in section 2 we summarize the main features of SCDFT and describe our computational approach; in sections 3–5 we present our results for Pb and H under pressure and CaBeSi, respectively; finally, in section 6, we summarize our conclusions.

2. The density functional theory for superconductors

Density functional theory [24] has enjoyed increasing popularity as a reliable and relatively inexpensive tool to describe real materials. In this section we will briefly outline the DFT approach to superconductivity, and refer to the original papers for more details. In order to give an introduction to SCDFT, it is instructive to recall how magnetism is treated within DFT. The Hohenberg–Kohn (HK) theorem [25] states that *all* observables, in particular also the magnetization, are functionals of the electronic density *alone*. This, however, assumes knowledge of the magnetization as a functional of the density. Finding an approximation for this functional is extremely hard and, in practice, one chooses a different approach. The task can be vastly simplified by treating the magnetization density $\mathbf{m}(\mathbf{r})$, i.e. the order parameter of the magnetic state, as an additional fundamental density in the density functional framework [26]. An auxiliary field—here a magnetic field $\mathbf{B}_{\rm ext}(\mathbf{r})$—is introduced, which couples to $\mathbf{m}(\mathbf{r})$ and breaks the corresponding (rotational) symmetry of the Hamiltonian. This field drives the system into the ordered state. If the system is actually magnetic, the order parameter will survive when the auxiliary perturbation is quenched. In this way, the ground-state magnetization density is determined by minimizing the total energy functional (free energy functional for finite temperature calculations) with respect to both the normal density and the magnetization density. Within this approach much simpler approximations to the xc functional (now a functional of two densities) can lead to satisfactory results.

The same idea is also at the heart of density functional theory for superconductors, as formulated by Oliveira *et al* [27]. Here the order parameter is the so-called anomalous density:

$$\chi(\mathbf{r}, \mathbf{r}') = \langle \hat{\Psi}_\uparrow(\mathbf{r}) \hat{\Psi}_\downarrow(\mathbf{r}') \rangle, \tag{1}$$

and the corresponding potential is the non-local pairing potential $\Delta(\mathbf{r}, \mathbf{r}')$. It can be interpreted as an external pairing field, induced by an adjacent superconductor via the proximity effect. Again, this external field only acts to break the symmetry (here the gauge symmetry) of the system, and is quenched at the end of the calculation. As in the case of magnetism, if the system is actually a superconductor the order parameter will be sustained by the self-consistent effective pairing field. The approach outlined so far captures, in principle, all the electronic degrees of freedom. To describe conventional phonon-mediated superconductors, the electron–phonon interaction also has to be taken into account.

In order to treat both weak and strong electron–phonon coupling, the electronic and the nuclear degrees of freedom have to be treated on an equal footing. This can be achieved by a multi-component DFT, based on both the electronic density and the diagonal of the nuclear N-body density matrix [28, 29][5]:

$$\Gamma(\underline{\mathbf{R}}) = \langle \hat{\Phi}^\dagger(\mathbf{R}_1) \cdots \hat{\Phi}^\dagger(\mathbf{R}_N) \hat{\Phi}(\mathbf{R}_N) \cdots \hat{\Phi}(\mathbf{R}_1) \rangle, \tag{2}$$

where $\hat{\Phi}(\mathbf{R})$ is a nuclear field operator. The quantity $\Gamma(\underline{\mathbf{R}})$ is then included as an additional 'density' in the formalism, besides the electronic density and the SC order parameter.

In order to formulate a Hohenberg–Kohn theorem for this system, we introduce a set of three potentials, which couple to the three densities described above. Since the electron–nuclear interaction, which in conventional DFT constitutes the external potential, is treated explicitly in this formalism, it is *not* part of the external potential. The nuclear Coulomb interaction $\hat{U}^{nn}$ already has the form of an external many-body potential, coupling to $\Gamma(\underline{\mathbf{R}})$, and for the sake of the Hohenberg–Kohn theorem this potential will be allowed to take the form of an arbitrary N-body potential. All three external potentials are merely mathematical devices, required to formulate a Hohenberg–Kohn theorem. At the end of the derivation, the external electronic and pairing potentials will be set to zero while the external nuclear many-body potential is set to the nuclear Coulomb interaction.

As usual, the Hohenberg–Kohn theorem guarantees a one-to-one mapping between the set of densities $\{n(\mathbf{r}), \chi(\mathbf{r}, \mathbf{r}'), \Gamma(\underline{\mathbf{R}})\}$ in thermal equilibrium and the set of their conjugate potentials $\{v^{\rm e}_{\rm ext}(\mathbf{r}) - \mu, \Delta_{\rm ext}(\mathbf{r}, \mathbf{r}'), v^{\rm n}_{\rm ext}(\underline{\mathbf{R}})\}$. Therefore all the observables are functionals of the set of densities. Finally, it

[5] Taking only the nuclear density would lead to a system of strictly non-interacting nuclei which obviously would give rise to non-dispersive, hence unrealistic, phonons.

ensures that the grand canonical potential

$$\Omega[n,\chi,\Gamma] = F[n,\chi,\Gamma] + \int \mathrm{d}^3r\, n(\mathbf{r})[v^{\mathrm{e}}_{\mathrm{ext}}(\mathbf{r}) - \mu] - \int \mathrm{d}^3r \int \mathrm{d}^3r'\, [\chi(\mathbf{r},\mathbf{r}')\Delta^*_{\mathrm{ext}}(\mathbf{r},\mathbf{r}') + \mathrm{h.c.}] + \int \mathrm{d}^3\underline{R}\, \Gamma(\underline{\mathbf{R}}) v^{\mathrm{n}}_{\mathrm{ext}}(\underline{\mathbf{R}}), \tag{3}$$

is minimized by the equilibrium densities. We use the notation $A[f]$ to denote that A is a functional of f. The functional $F[n,\chi,\Gamma]$ is universal in the sense that it does not depend on the external potentials. It is defined by

$$F[n,\chi,\Gamma] = T^{\mathrm{e}}[n,\chi,\Gamma] + T^{\mathrm{n}}[n,\chi,\Gamma] + U^{\mathrm{en}}[n,\chi,\Gamma] + U^{\mathrm{ee}}[n,\chi,\Gamma] - \frac{1}{\beta}S[n,\chi,\Gamma], \tag{4}$$

where T^{e} represents the electronic kinetic energy, U^{ee} the electron–electron interaction, T^{n} the nuclear kinetic energy, U^{nn} the Coulomb repulsion between nuclei, U^{en} the electron–nuclei interaction and S the entropy of the system:

$$S[n,\chi,\Gamma] = -\mathrm{Tr}\{\hat{\rho}_0[n,\chi,\Gamma]\ln(\hat{\rho}_0[n,\chi,\Gamma])\}. \tag{5}$$

In standard DFT one normally defines a Kohn–Sham system, i.e. a non-interacting system chosen such that it has the same ground-state density as the interacting one. The variational procedure for this system gives Schrödinger-like (Kohn–Sham) equations for non-interacting electrons subject to an effective (Kohn–Sham) potential. These equations are nowadays routinely solved by solid state theorists. In our formalism, the Kohn–Sham system consists of non-interacting (superconducting) electrons and *interacting* nuclei. We will not describe here the details of the method and will only outline its basic features: the Kohn–Sham potentials, which are derived in analogy to normal DFT, include the external fields, Hartree and exchange–correlation terms. The latter account for all many-body effects of the electron–electron and electron–nuclear interactions. Obtaining their explicit form has represented a major theoretical effort [30–32]. Once this problem has been solved, the problem of minimizing the Kohn–Sham grand canonical potential can be transformed into a set of three differential equations that have to be solved self-consistently: one equation for the nuclei, which resembles the familiar nuclear Born–Oppenheimer equation, and two coupled equations which describe the electronic degrees of freedom and have the algebraic structure of the Bogoliubov–de Gennes [33] equations.

The resulting Kohn–Sham Bogoliubov–de Gennes (KS–BdG) equations are (we use atomic hartree units)

$$\left[-\frac{\nabla^2}{2} + v^{\mathrm{e}}_{\mathrm{s}}(\mathbf{r}) - \mu\right] u_{n\mathbf{k}}(\mathbf{r}) + \int \mathrm{d}^3r'\, \Delta_{\mathrm{s}}(\mathbf{r},\mathbf{r}') v_{n\mathbf{k}}(\mathbf{r}') = \tilde{E}_{n\mathbf{k}}\, u_{n\mathbf{k}}(\mathbf{r}), \tag{6a}$$

$$-\left[-\frac{\nabla^2}{2} + v^{\mathrm{e}}_{\mathrm{s}}(\mathbf{r}) - \mu\right] v_{n\mathbf{k}}(\mathbf{r}) + \int \mathrm{d}^3r'\, \Delta^*_{\mathrm{s}}(\mathbf{r},\mathbf{r}') u_{n\mathbf{k}}(\mathbf{r}') = \tilde{E}_{n\mathbf{k}}\, v_{n\mathbf{k}}(\mathbf{r}), \tag{6b}$$

where $u_{n\mathbf{k}}(\mathbf{r})$ and $v_{n\mathbf{k}}(\mathbf{r})$ are the particle and hole amplitudes. This equation is very similar to the Kohn–Sham equations in the OGK formalism [27]. However, in the present formulation the lattice potential is not considered an external potential but enters via the electron–ion Hartree term. Furthermore, our exchange–correlation potentials depend on the nuclear density matrix, and therefore on the phonons. Although equations (6) and the corresponding equation for the nuclei have the structure of static mean-field equations, they contain, in principle, all correlation and retardation effects through the exchange–correlation potentials.

These KS–BdG equations can be simplified by the so-called decoupling approximation [13, 34], which corresponds to approximating the particle and hole amplitudes by

$$u_{n\mathbf{k}}(\mathbf{r}) \approx u_{n\mathbf{k}}\varphi_{n\mathbf{k}}(\mathbf{r}); \qquad v_{n\mathbf{k}}(\mathbf{r}) \approx v_{n\mathbf{k}}\varphi_{n\mathbf{k}}(\mathbf{r}), \tag{7}$$

where the wavefunctions $\varphi_{n\mathbf{k}}(\mathbf{r})$ are the solutions of the normal Schrödinger equation. In this way the eigenvalues in equations (6) become $\tilde{E}_{n\mathbf{k}} = \pm E_{n\mathbf{k}}$, where

$$E_{n\mathbf{k}} = \sqrt{\xi^2_{n\mathbf{k}} + |\Delta_{n\mathbf{k}}|^2}, \tag{8}$$

and $\xi_{n\mathbf{k}} = \epsilon_{n\mathbf{k}} - \mu$. This form of the eigenenergies allows us to interpret the pair potential $\Delta_{n\mathbf{k}}$ as the gap function of the superconductor. Furthermore, the coefficients $u_{n\mathbf{k}}$ and $v_{n\mathbf{k}}$ are given by simple expressions within this approximation:

$$u_{n\mathbf{k}} = \frac{1}{\sqrt{2}}\mathrm{sgn}(\tilde{E}_{n\mathbf{k}})\mathrm{e}^{\mathrm{i}\phi_{n\mathbf{k}}}\sqrt{1 + \frac{\xi_{n\mathbf{k}}}{\tilde{E}_{n\mathbf{k}}}}, \tag{9a}$$

$$v_{n\mathbf{k}} = \frac{1}{\sqrt{2}}\sqrt{1 - \frac{\xi_{n\mathbf{k}}}{\tilde{E}_{n\mathbf{k}}}}. \tag{9b}$$

Finally, the matrix elements $\Delta_{n\mathbf{k}}$ are defined as

$$\Delta_{n\mathbf{k}} = \int \mathrm{d}^3r \int \mathrm{d}^3r'\, \varphi^*_{n\mathbf{k}}(\mathbf{r})\Delta_{\mathrm{s}}(\mathbf{r},\mathbf{r}')\varphi_{n\mathbf{k}}(\mathbf{r}'), \tag{10}$$

and $\phi_{n\mathbf{k}}$ is the phase $\mathrm{e}^{\mathrm{i}\phi_{n\mathbf{k}}} = \Delta_{n\mathbf{k}}/|\Delta_{n\mathbf{k}}|$. The normal and anomalous densities can then be easily obtained from

$$n(\mathbf{r}) = \sum_{n\mathbf{k}}\left[1 - \frac{\xi_{n\mathbf{k}}}{E_{n\mathbf{k}}}\tanh\left(\frac{\beta}{2}E_{n\mathbf{k}}\right)\right]|\varphi_{n\mathbf{k}}(\mathbf{r})|^2 \tag{11a}$$

$$\chi(\mathbf{r},\mathbf{r}') = \frac{1}{2}\sum_{n\mathbf{k}}\frac{\Delta_{n\mathbf{k}}}{E_{n\mathbf{k}}}\tanh\left(\frac{\beta}{2}E_{n\mathbf{k}}\right)\varphi_{n\mathbf{k}}(\mathbf{r})\varphi^*_{n\mathbf{k}}(\mathbf{r}'). \tag{11b}$$

Within the decoupling approximation, we finally arrive at an equation for the **k**-resolved superconducting gap $\Delta_{n\mathbf{k}}$, which has the following form [13, 14, 27, 35]:

$$\Delta_{n\mathbf{k}} = -\mathcal{Z}_{n\mathbf{k}}\Delta_{n\mathbf{k}} - \frac{1}{2}\sum_{n'\mathbf{k}'}\mathcal{K}_{n\mathbf{k},n'\mathbf{k}'}\frac{\tanh\left(\frac{\beta}{2}E_{n'\mathbf{k}'}\right)}{E_{n'\mathbf{k}'}}\Delta_{n'\mathbf{k}'}. \tag{12}$$

Equation (12) is the central equation of the DFT for superconductors. The kernel $\mathcal{K}$ consists of two contributions $\mathcal{K} = \mathcal{K}^{\mathrm{e\text{-}ph}} + \mathcal{K}^{\mathrm{e\text{-}e}}$, representing the effects of the e–ph and the e–e interactions, respectively. The diagonal term $\mathcal{Z}$ plays a similar role as the renormalization term in the Eliashberg equations. Explicit expressions of $\mathcal{K}^{\mathrm{e\text{-}ph}}$ and $\mathcal{Z}$, which are the results of the approximate functionals, are given in equations 9

and 11 of [14], respectively. These two terms involve the e–ph coupling matrix, while $\mathcal{K}^{e\text{-}e}$ contains the matrix elements of the screened Coulomb interaction. Equation (12) has the same structure as the BCS gap equation, with the kernel $\mathcal{K}$ replacing the model interaction of BCS theory. This similarity allows us to interpret the kernel as an effective interaction responsible for the binding of the Cooper pairs. Moreover, we emphasize that equation (12) is not a mean-field equation (as in BCS theory), since it contains correlation effects via the SC exchange–correlation functional entering $\mathcal{K}$ and $\mathcal{Z}$. Furthermore, it has the form of a static equation—i.e. it does not depend *explicitly* on the frequency—and therefore has a simpler (and computationally more manageable) structure than the Eliashberg equations. However, this certainly does not imply that retardation effects are absent from the theory. Once again, retardation effects enter through the xc functional, as explained in [13, 14]. The SCDFT allows us to treat the e–ph and the screened e–e interactions on the same footing. These terms, however, can be treated at different levels of approximation.

We calculated the screened Coulomb matrix elements (ME) with respect to the Bloch functions for the whole energy range of relevant valence and conduction states. The different nature of the electronic bands in each material (e.g. some of them can be highly localized while others are more delocalized) strongly calls for the use of a non-diagonal screening, including local field effects.

As mentioned above, the normal-state calculations, necessary for the study of the superconducting state, are performed within DFT in the LDA or GGA approximations. Computationally, the electronic and phononic properties are obtained using the pseudopotential method as implemented in the QUANTUM-ESPRESSO package [36]; the screened Coulomb matrix elements are obtained with the SELF [37] code.

3. Multiband superconductivity in Pb

The peculiar aspects of superconductivity in Pb have been discussed in the past [5–7, 17, 18, 38–40]. In this section we present the results for the SC properties of Pb, calculated within the SCDFT formalism, and highlight the importance of the $(n, \mathbf{k})$ gap anisotropy in this system. We first concentrate on the SC gap function, i.e. the solution of equation (12). There are two ways to visualize this function: the first is to look at the gap as a function of the normal-state energy eigenvalue. The set of black points in figure 1 shows the gap at $T = 0$ K calculated on a set of random $\mathbf{k}$ points as a function of the energy distance from the Fermi level E_F. An important feature of this plot is that, for each energy, the gap is not a single-valued function. This means that, in general, the SC gap is not isotropic in reciprocal space, i.e. for $\varepsilon = E_F$ its value depends on the Fermi vector $\mathbf{k}_F$. In particular, for each $\varepsilon \approx E_F$ we observe two distinct 'sets' of gaps, in strict analogy with the case of MgB_2 (see, for comparison, figure 1 in [12]). Moreover, each 'set' has an associated, finite, vertical energy spread.

Most importantly the gap function has a negative tail extending to high energy. This is a general feature of the gap function, due to the presence of the Coulomb repulsion and to its dominance for large energies. Due to this feature, Coulomb renormalization effects are properly included in the SCDFT formalism. We emphasize that these effects are crucial to obtain a predictive superconducting solution.

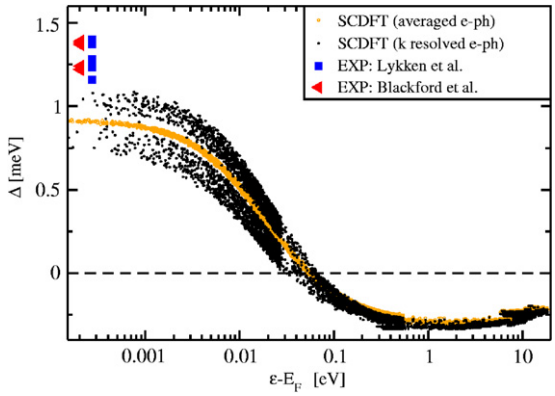

Figure 1. Superconducting gap of Pb as a function of the energy distance from the Fermi energy ($T = 0$ K). Small black points: Δ resulting from the inclusion of the $\mathbf{k}$-resolved e–ph and Coulomb matrix elements. Small orange points: Δ calculated with a corresponding averaged e–ph interaction (Eliashberg function $\alpha^2F(\Omega)$). Large triangles and squares: experimental values (from [17, 18]).

A second possibility to visualize the gap is to define equi-energy surfaces and plot the gap value on that surface. The equi-energy surface can be chosen to be the Fermi surface (FS). In figure 2(a) we plot the FS of Pb, consisting of two separate sheets, coming from the two (essentially p) bands crossing E_F. The sheets are topologically quite different, the first one being rather spherical and the second having a more complex tubular-like structure. The colors σ in figure 2(a) represents the values of $\Delta_{n\mathbf{k}_F}$. It is clear that the two distinct sets of Δ in figure 1 come from the two sheets of the Fermi surface. Figure 1 shows that their energy separation is in good agreement with the experiments [17, 18].

Figure 2(a) also shows that $\Delta_{n\mathbf{k}}$ is anisotropic inside each single sheet, resulting in the vertical energy spread mentioned before (intra-bandgap anisotropy). Continuing our analysis, in figure 2(b) we plot the e–ph coupling $\lambda_{n\mathbf{k}_F}$ on the FS, where

$$\lambda_{n\mathbf{k}} = 2\sum_{n'\mathbf{k}',\nu} \frac{|g^{nn'}_{\mathbf{k},\mathbf{k}',\nu}|^2}{\omega_{\mathbf{k}'-\mathbf{k},\nu}} \times \delta(\varepsilon_{n'\mathbf{k}'} - E_F) \qquad (13)$$

is the average of all possible e–ph scattering processes connecting two points at FS, but always involving the electronic initial state $(n, \mathbf{k})$. The total e–ph coupling constant λ can be expressed as $\lambda = \frac{1}{N(E_F)}\sum_{n\mathbf{k}} \lambda_{n\mathbf{k}}\delta(\varepsilon_{n\mathbf{k}} - E_F)$. Comparing the plots in figures 2(a) and (b) we notice a striking similarity, which indicates a strong correlation between the n dependence and $\mathbf{k}$ anisotropy of the e–ph coupling and of the gap. This is a general feature that we also observe for other materials. Moreover, our calculations show that the gap anisotropy is due to the e–ph coupling only: the orange points in figure 1 show the gap function calculated with an average e–ph interaction, i.e. including the phononic kernels $\mathcal{K}^{e\text{-}ph}$

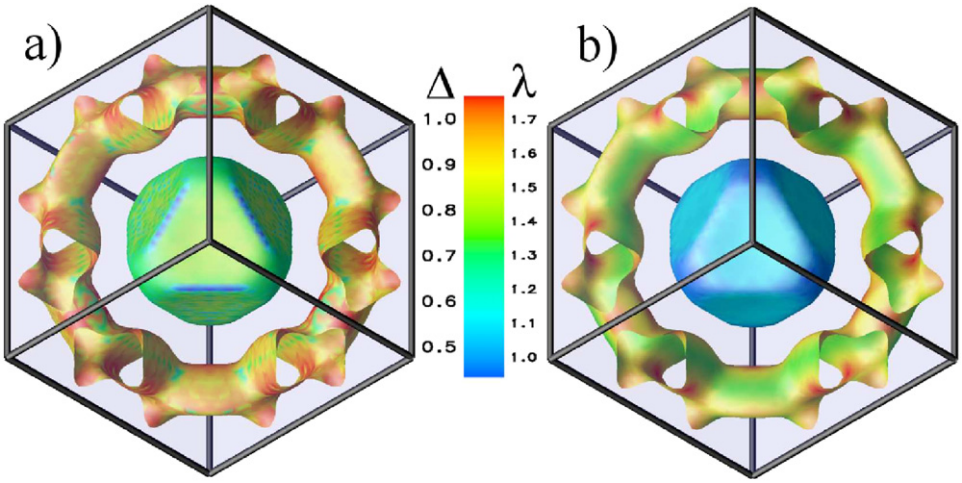

Figure 2. (a) (Left): superconducting gap $\Delta_{n\mathbf{k}}$ calculated at the Fermi surface of Pb at $T = 0$ K. (b) (Right): electron–phonon interaction $\lambda_{n\mathbf{k}}$ at FS.

and $\mathcal{Z}$ that contain the Eliashberg function $\alpha^2F(\Omega)$ (see equations 23 and 24 of [14]), but still with the Coulomb ME $\mathcal{K}^{\text{e-e}}_{n\mathbf{k},n'\mathbf{k}'}$. It is clear that the e–ph average washes out all the band and **k** dependence of the gap (i.e. $\Delta_{n\mathbf{k}} = \Delta(\varepsilon_{n\mathbf{k}})$).

Equation (12) allows us to calculate $\Delta_{n\mathbf{k}}$ as a function of temperature T, defining T_c from the condition that $\Delta_{n\mathbf{k}}(T_c) = 0$. We obtain $T_c = 5.25$ K and $T_c = 4.84$ K for the anisotropic and average calculation, respectively. We see that, although certainly not in a proportion comparable with MgB_2, the presence of an anisotropic, multiband gap produces an 8% enhancement of the value of T_c. In MgB_2 this effect is much more pronounced [9–12] than in the present case. This is partially due to the much lower difference in e–ph coupling between the two bands (in MgB_2 the coupling in the σ bands is roughly three times higher than in the π bands).

An interesting question is under which conditions does a system show multiband superconductivity, i.e. with a clear separation between the gaps. Looking again at the $\lambda_{n\mathbf{k}_F}$ we see that in Pb the two sets corresponding to the two bands crossing E_F are not continuous, i.e. the values of $\lambda_{1\mathbf{k}_F}$ and $\lambda_{2\mathbf{k}_F}$ do not superimpose. In order to check whether the presence of two separate gaps is related directly to this property of the $\lambda_{n\mathbf{k}_F}$, we performed several model calculations, rescaling the e–ph ME, in order to have a continuous set of $\lambda_{n\mathbf{k}_F}$ *and* keeping constant the value of the total average λ. Most interestingly we found that the two SC gaps $\Delta_{n\mathbf{k}_F}$ become continuous exactly when the two sets of $\lambda_{n\mathbf{k}_F}$ do, independent of the details of how the coupling was modified to bring the $\lambda_{n\mathbf{k}_F}$ to merge. This leads us to conclude that Pb is a two-gap system due to the fact that $\lambda_{n\mathbf{k}_F}$ are disjoint sets (relative to the band n). In general there are two necessary conditions to fulfill in order to obtain multigap superconductivity. First, the system needs to have disconnected FS sheets, and second the electron–phonon coupling must be different on each of these sheets.

4. Superconductivity in H under pressure

Based on the simple BCS theory of superconductivity, we can understand why molecular metallic hydrogen could be a good superconductor [20]: this system has very high phonon frequencies due to the light H mass, and it has a possibly strong electron–phonon interaction related to the lack of core electrons and to the quite strong covalent bonding within the H_2 molecules. Many studies, aiming at investigating further this possibility [41–43], collected strong evidence pointing to high-T_c superconductivity. At present, however, the full scenario is still far from being clear and well established.

The low temperature and high pressure (>400 GPa) phase of molecular hydrogen is predicted to be a base-centered orthorhombic metallic molecular solid (known as a *Cmca* phase [44]) with two molecules per unit cell located on different layers. The electronic band structure arises from the bonding and anti-bonding combination of the H_2 molecular orbitals. At high pressure, the band overlap between the valence and conduction bands produces a rich and complex Fermi surface (figure 3) with disconnected sheets of different orbital nature [45] and provides the strong e–ph coupling necessary for superconductivity (see below).

Three types of bands form the Fermi surface of H at high pressure: the two tubular structures intersecting the k_y axis and the two prism-like structures along the k_x axis have hole-type character; the disc centered at the Γ-point and the structures near the C-point have electron-type character; the remaining sheets are related to degenerate orbitals along Z–T. The different orbital character of the FS branches suggests the occurrence of different couplings between the various bands, leading to an anisotropic SC gap and to multiband superconductivity.

The molecular nature of the charge density distribution gives rise to an intriguing phonon dispersion (figure 4). The phonon modes can be grouped into three main branches: phononic, libronic and vibronic, corresponding respectively to the relative translations, rotations and internal vibrations of the H_2 molecules. The three FS regions possess distinct e–ph coupling: the most coupled one is the disc at Γ with $1.8 < \lambda_{\mathbf{k}} < 2.00$; then, we find the two prism-like structures with $1.00 < \lambda_{\mathbf{k}} < 1.80$ and the other sheets with $\lambda_{\mathbf{k}} < 1.00$. The tubular structures have the smallest $\lambda_{\mathbf{k}}$. The presence of

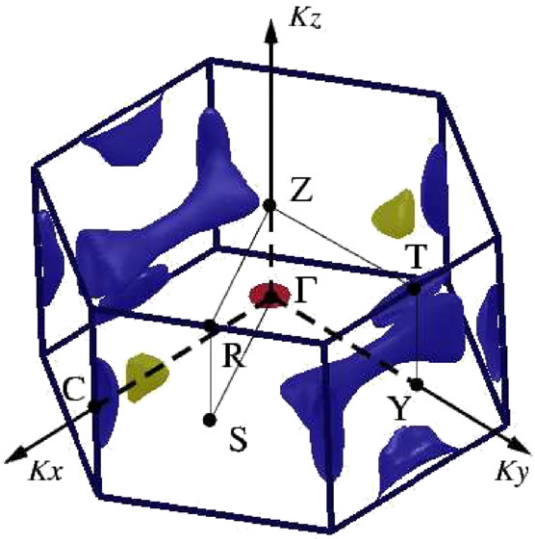

Figure 3. Fermi surface at 414 GPa. Different colors represent different values of the superconducting gap on the FS. Red (18.0 meV $<\Delta<$ 21 meV), yellow (13.6 meV $<\Delta<$ 18.0 meV) and blue (10.0 meV $<\Delta<$ 13.6 meV).

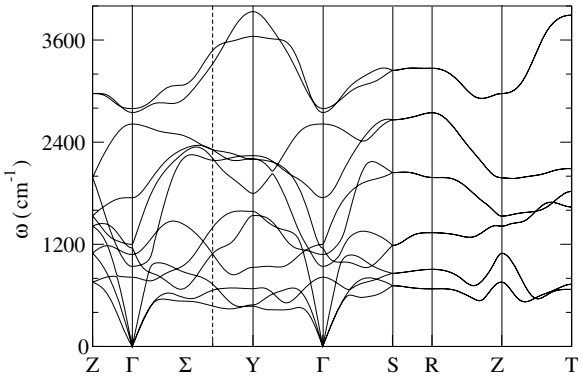

Figure 4. H phonon dispersion at 414 GPa.

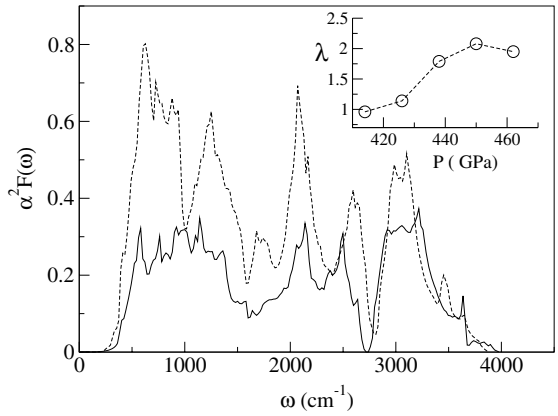

Figure 5. $\alpha^2F(\Omega)$ at 414 (solid line) and 462 (dashed line) GPa. The inset shows the electron–phonon coupling (λ) as a function of the pressure.

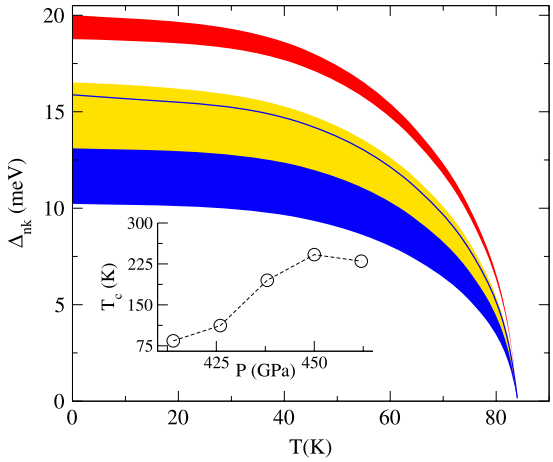

Figure 6. $\Delta_{n\mathbf{k}}$ at E_F at 414 GPa. The shaded regions represent the **k** anisotropy over different bands (note that the blue and yellow gaps overlap from 13.00 to 15.75 meV). The inset shows the superconducting critical temperature as a function of pressure.

multiple Fermi surfaces provides a '**q**-distributed' coupling, with many modes contributing to the pairing. This allows us to increase λ still avoiding a lattice instability, which could result from very high coupling at some specific **q**s. In fact, the Eliashberg function (figure 5) shows three main frequency regions *all* of them strongly coupled to the electrons and associated with phononic, libronic and vibronic modes, in an increasing frequency order. However, a net distinction between phononic and libronic modes (in the low frequency region: 0 cm^{-1} $\leqslant \omega \leqslant$ 1600 cm^{-1}) is prevented due to the branch mixing caused by the large renormalization of the libronic modes. As the pressure increases from 414 GPa, the coupling increases and a new feature appears at $\approx$1700 cm^{-1} (figure 5, plot at 462 GPa). The additional peak in the $\alpha^2F(\omega)$ comes from an extra band which crosses the Fermi level close to the R point. This creates a new electron-like Fermi sheet, strongly coupled with in-phase libronic modes, and opens a further coupling channel at higher pressure, giving rise to a jump of λ at $\approx$435 GPa (inset of figure 5).

Although rather large, these values of λ are of the same order as, for example, those obtained in fcc-Li under high pressure (40 GPa). There, T_c reached $\simeq$20 K, a very large value for a free-electron-like metal. In the case of hydrogen, we expect that the large phonon frequencies provided by the H_2 vibronic modes lead to much higher T_cs.

The T_c was calculated by solving the SCDFT anisotropic gap equation (12). As previously shown in the case of low-density metals [15] and discussed by Richardson and Ashcroft [46] a complete inclusion of both electron–phonon and electron–electron interactions is crucial to reproduce the experimental T_cs. We find very high T_cs, considerably increasing with pressure up to 242 K at 450 GPa (inset of figure 6). Comparing figures 5 and 6 insets, it is clear that T_c follows closely the λ behavior with pressure.

We predict a multigap (three-gap) superconductivity, which is progressively lost at high pressure, where inter-band scattering increases the non-diagonal matrix elements, leading to a merging of the different gaps. The occurrence of multigap superconductivity is clearly illustrated in figure 6, which shows

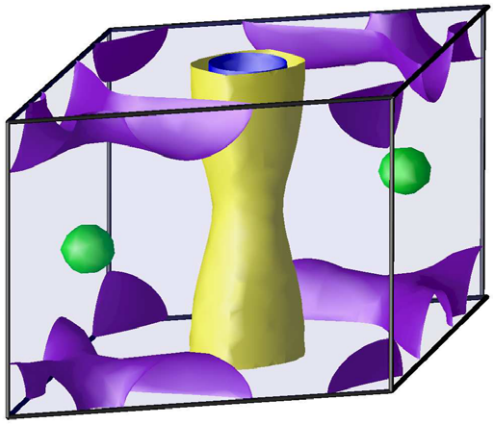

Figure 7. CaBeSi Fermi surface. The colors identify the three gaps at E_F: the largest σ (yellow and blue cylindrical-like sheets); the intermediate π bonding (green spheres); the lowest π anti-bonding (violet).

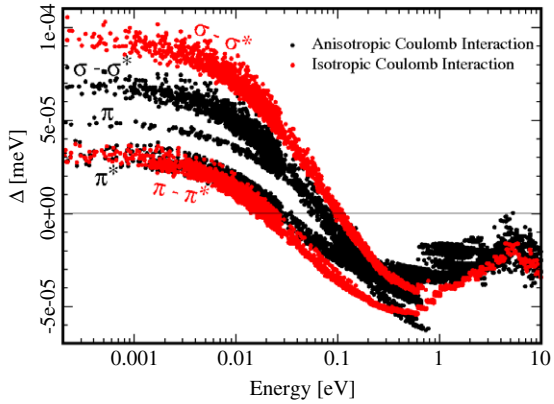

Figure 8. CaBeSi superconducting gap as a function of the energy distance from the Fermi level.

the $\Delta_{n\mathbf{k}}$ at the Fermi level as a function of temperature (for all the bands (n) and $\mathbf{k}$ points) and at the pressure with largest band anisotropy, $P = 414$ GPa ($T_c = 84$ K). The three gaps are evident: the largest one at ≈19.3 meV and two very anisotropic overlapping gaps at 15.4 and 13.6 meV. The three gaps are associated with the three different FS sheets (cf figure 3): the strongly coupled disc around the Γ-point, the prism-like sheets and others associated with the lowest gap.

In H the main source of band anisotropy is given by the e–ph interaction. Furthermore a simple multigap BCS model (not including anisotropy in $\mathbf{k}$), although not adequate to treat a strong coupling system, is able to reproduce qualitatively the full SCDFT results [47]. This suggests that the dominant effect of the anisotropy on T_c is related to the band contribution and that the $\mathbf{k}$ space anisotropy is less relevant. We emphasize, however, that, although the anisotropy of the interaction generates three different gaps, it does not play a fundamental role in enhancing T_c, which shows an increase of only 10 K compared to the value obtained within an isotropic approximation. This is due to the fact that in H the inter-band (low-$\mathbf{q}$) coupling dominates over the intra-band coupling (high-$\mathbf{q}$) [47]. This is different from MgB_2, where the intra-band coupling is much stronger and the anisotropy doubles the critical temperature [10, 12].

5. Superconductivity in CaBeSi

In this section we report the SC properties of $CaBe_xSi_{2-x}$ at $x = 1$ (CaBeSi in the following) in the AlB_2 phase, with Be and Si atoms alternating within the honeycomb layers with an AA stacking. A general similarity is found between CaBeSi and MgB_2: in both materials the σ, π-bonding (π_b) and π-anti-bonding (π_a) bands cross the Fermi level (E_F). In CaBeSi the π_b bands are almost fully occupied, leaving only small hole pockets at K which give rise to the little π spheres of the Fermi surface (figure 7). These replace the π tubular structure present in MgB_2.

Despite the general similarities, CaBeSi and MgB_2 have rather different chemical and phononic properties, with important consequences for the e–ph interaction [22]. In fact, CaBeSi phonon frequencies are lower in comparison with MgB_2, mainly due to the larger mass of Ca and Si versus Mg and B. In the CaBeSi phonon dispersion, the E_{2g} mode is fairly flat along the in-plane BZ symmetry lines and it shows only a very weak renormalization (four times smaller than in MgB_2 [48–50]) due to the very small E_{2g} electron–phonon matrix elements. In turn, this is related to the delocalized and ionic nature of the σ bonds in CaBeSi. In fact, the connection between strongly covalent bonds and strong e–ph coupling seems to be a general feature [15, 16, 19, 51]. The small e–ph coupling makes CaBeSi a weak coupling superconductor with e–ph $\lambda = 0.38$ and $T_c = 0.4$ K, in spite of a nesting at the Fermi surface twice as large as in MgB_2.

The solution of the self-consistent gap equation reveals an unexpected complex structure (figure 8) with three clearly separated gaps at E_F (unlike in H where two of the three gaps superpose). The calculated critical temperature is very low ($T_c = 0.4$), lower than the upper limit (4.2 K) set by the experimental results [23]. Unlike in MgB_2, where superconductivity is interpreted within a two-band model [9, 52–54], in CaBeSi there is a further π_b–π_a gap splitting. As in MgB_2, the largest gap is related to the σ FS sheets (cylindrical-like structures in figure 7), the intermediate one to π_b sheets (small hole spheres) and the lowest to π_a sheets. The additional π_b–π_a gap splitting is a peculiar feature of CaBeSi not present in MgB_2, where the two σ and the two π gaps merge together. In order to understand the origin of this splitting we perform some additional computational experiments, solving the gap equation (i) completely neglecting the Coulomb interaction, (ii) including only an averaged Coulomb term and (iii) with isotropically averaged Coulomb and phononic interactions, corresponding to the dirty limit. In both (i) and (ii) cases, the three-gap structure is destroyed, bringing back a two-band, MgB_2-like gap structure. In case (iii), instead, superconductivity is completely lost. As a result, we predict superconductivity in CaBeSi *only* if the anisotropic structure of the interactions is included. While, as in MgB_2, the σ–π gap splitting is related to the different e–ph coupling in these bands, the further π_b–π_a splitting is a pure effect of the complex structure of the

anisotropic Coulomb repulsion, acting in a different way on the π_b and π_a states.

6. Summary

Three multigap superconductors were investigated in this work: Pb and H under pressure, and CaBeSi. Without assuming any ad hoc model or adjustable parameters, we find that Pb is a two-gap superconductor, in agreement with available experiments and with previous theoretical results based on other methods. We show that the n and **k** gap anisotropy and the separation of the two gaps correlate strongly with the anisotropy of the electron–phonon interaction on the different sheets of the Fermi surface. This multigap character produces an enhancement of T_c relative to the isotropic case.

For H, we find a strong increase of the critical temperature with increasing pressure. As the corresponding pressure regime is not yet experimentally accessible our calculation of the astonishingly high critical temperatures represents a genuine prediction. The analysis of the electronic and phononic properties points to the origins of the strong enhancement of superconductivity with rising pressure: in particular (i) we confirm a strong electron–phonon coupling, increasing with pressure and (ii) the presence of multiple Fermi surfaces with different character provides both strong intra-band (low-**q**) and inter-band (high-**q**) electron–phonon scattering. In this respect, (iii) a major role is played by the molecular rotational (libronic) and vibrational (vibronic) modes, which are strongly coupled with the inter-molecular charge. Finally, (iv) we predict three superconducting gaps at the Fermi level, associated with Fermi surface branches having different character.

We have also investigated the superconducting properties of CaBeSi, a material isostructural and isoelectronic to MgB_2. While the band structures present strong similarities, the phonon structure and the e–ph interaction of the two systems differ substantially. In particular, the less localized σ charge of CaBeSi leads to a dramatic reduction in the E_{2g} electron–phonon coupling, with a consequent reduction of the phonon renormalization seen in MgB_2. Interestingly, CaBeSi exhibits three superconducting gaps at the Fermi level. The π_b–π_a splitting is a pure effect of the complex structure of the anisotropic Coulomb repulsion, acting differently on the π_b and π_a states.

The role of multigap superconductivity in enhancing the critical temperature of superconducting materials has been known for a long time. However, the crucial challenge is to predict under which circumstances and for which materials the phenomenon of multigap superconductivity actually occurs. With the SCDFT approach which features a fully anisotropic description of the electron–phonon coupling and of the screened Coulomb repulsion on an *ab initio* basis, this goal has been achieved.

Acknowledgments

This work makes use of results produced by the Cybersar Project managed by the Consorzio COSMOLAB, co-funded by the Italian Ministry of University and Research (MUR) within the Programma Operativo Nazionale 2000–2006 'Ricerca Scientifica, Sviluppo Tecnologico, Alta Formazione' per le Regioni Italiane dellObiettivo 1 Asse II, Misura II.2 Societ dellInformazione. This work was partially supported by the Italian Ministry of Education through PRIN 200602174 project, by INFM-CNR through a supercomputing grant at Cineca (Bologna, Italy), by the Deutsche Forschungsgemeinschaft within SPP1145 and by NANOQUANTA Network of Excellence of the European Union.

References

[1] Suhl H, Matthias B T and Walker L R 1959 BCS theory of superconductivity in the case of overlapping bands *Phys. Rev. Lett.* **3** 552
[2] Shen L Y L, Senozan N M and Phillips N E 1965 Evidence for two energy gaps in high-purity superconducting Nb, Ta, and V *Phys. Rev. Lett.* **14** 1025
[3] Radebaugh R and Keesom P H 1966 Low-temperature thermodynamic properties of vanadium. I. Superconducting and normal states *Phys. Rev.* **149** 209
[4] Binnig G, Baratoff A, Hoenig H E and Bednorz J G 1980 Two-band superconductivity in Nb-doped SrTiO3 *Phys. Rev. Lett.* **45** 1352
[5] Bennett A J 1965 Theory of the anisotropic energy gap in superconducting lead *Phys. Rev.* A **140** 1902
[6] Tomlinson P G and Carbotte J P 1976 Anisotropic superconducting energy gap in Pb *Phys. Rev.* B **13** 4738
[7] Short J D and Wolfe J P 2000 Evidence for large gap anisotropy in superconducting Pb from phonon imaging *Phys. Rev. Lett.* **85** 5198
[8] Zavaritskii N V 1963 *Zh. Eksp. Teor. Fiz.* **45** 1839 Zavaritskii N V 1964 *Sov. Phys.—JETP* **18** 1260 (Engl. Transl.)
[9] Liu A Y, Mazin I I and Kortus J 2001 Beyond Eliashberg superconductivity in MgB2: anharmonicity, two-phonon scattering, and multiple gaps *Phys. Rev. Lett.* **87** 087005
[10] Choi H J, Roundy D, Sun H, Cohen M L and Louie S G 2002 First-principles calculation of the superconducting transition in MgB2 within the anisotropic Eliashberg formalism *Phys. Rev.* B **66** 020513
[11] Choi H J, Roundy D, Sun H, Cohen M L and Louie S G 2002 The origin of the anomalous superconducting properties of MgB2 *Nature* **418** 758
[12] Floris A, Profeta G, Lathiotakis N N, Lüders M, Marques M A L, Franchini C, Gross E K U, Continenza A and Massidda S 2005 Superconducting properties of MgB2 from first principles *Phys. Rev. Lett.* **94** 037004
[13] Lüders M, Marques M A L, Lathiotakis N N, Floris A, Profeta G, Fast L, Continenza A, Massidda S and Gross E K U 2005 *Ab initio* theory of superconductivity. I. Density functional formalism and approximate functionals *Phys. Rev.* B **72** 024545
[14] Marques M A L, Lüders M, Lathiotakis N N, Profeta G, Floris A, Fast L, Continenza A, Gross E K U and Massidda S 2005 *Ab initio* theory of superconductivity. II. Application to elemental metals *Phys. Rev.* B **72** 024546
[15] Profeta G, Franchini C, Lathiotakis N N, Floris A, Sanna A, Marques M A L, Lüders M, Massidda S, Gross E K U and Continenza A 2006 Superconductivity in lithium, potassium, and aluminum under extreme pressure: a first-principles study *Phys. Rev. Lett.* **96** 047003
[16] Sanna A, Franchini C, Floris A, Profeta G, Lathiotakis N N, Lüders M, Marques M A L, Gross E K U, Continenza A and Massidda S 2006 *Ab initio* prediction of pressure-induced superconductivity in potassium *Phys. Rev.* B **73** 144512

[17] Blackford B L and March R H 1969 Tunneling investigation of energy-gap anisotropy in superconducting bulk Pb *Phys. Rev.* **186** 397
[18] Lykken G I, Geiger A L, Dy K S and Mitchell E N 1971 Measurement of the superconducting energy gap and Fermi velocity in single-crystal lead films by electron tunneling *Phys. Rev.* B **4** 1523
[19] Floris A, Sanna A, Massidda S and Gross E K U 2007 Two-band superconductivity in Pb from *ab initio* calculations *Phys. Rev.* B **75** 054508
[20] Ashcroft N W 1968 Metallic hydrogen: a high-temperature superconductor? *Phys. Rev. Lett.* **21** 1748
[21] Ashcroft N W 2004 Bridgman's high-pressure atomic destructibility and its growing legacy of ordered states *J. Phys.: Condens. Matter* **16** S945
[22] Bersier C, Floris A, Sanna A, Profeta G, Continenza A, Gross E K U and Massidda S 2009 Electronic, dynamical and superconducting properties of CaBeSi *Phys. Rev.* B at press
(Bersier C, Floris A, Sanna A, Profeta G, Continenza A, Gross E K U and Massidda S 2008 arXiv:0803.1044)
[23] Sano F, Takahashi Y, Takase K, Takano Y and Sekizawa K 2006 *CP850 Low Temperature Physics: 24th Int. Conf. on Low Temperature Physics*
[24] Dreizler R M and Gross E K U 1990 *Density Functional Theory* (Berlin: Springer)
[25] Hohenberg P and Kohn W 1964 Inhomogeneous electron gas *Phys. Rev.* B **136** 864
[26] Vonbarth U and Hedin L 1972 A local exchange–correlation potential for the spin polarized case *J. Phys. C: Solid State Phys.* **5** 1629
[27] Oliveira L N, Gross E K U and Kohn W 1988 Density functional theory for superconductors *Phys. Rev. Lett.* **70** 2430
[28] Kreibich T and Gross E K U 2001 Multicomponent density-functional theory for electrons and nuclei *Phys. Rev. Lett.* **86** 2984
[29] Kreibich T, van Leeuwen R and Gross E K U 2008 Multicomponent density-functional theory for electrons and nuclei *Phys. Rev.* A **78** 022501
[30] Kurth S Exchange-correlation functionals for inhomogeneous superconductors *PhD Thesis* Julius-Maximilians-Universität Würzburg http://www.physik.fu-berlin.de/∼ag-gross/theses/kurth_phd.pdf
[31] Lüders M Density functional theory for superconductors: a first principles approach to the superconducting phase *PhD Thesis* Julius-Maximilians-Universität Würzburg http://www.physik.fu-berlin.de/∼ag-gross/theses/lueders_phd.pdf
[32] Marques M M Density functional theory for superconductors: exchange and correlation potentials for inhomogeneous systems *PhD Thesis* Julius-Maximilians-Universität Würzburg http://www.physik.fu-berlin.de/∼ag-gross/theses/marques_phd.pdf
[33] Bogoliubov N N, Tolmachov V V and Širkov D V 1958 A new method in the theory of superconductivity *Fortschr. Phys.* **6** 605
[34] Gross E K U and Kurth S 1991 Density functional theory of the superconducting state *Int. J. Quantum Chem. Symp.* **25** 289
[35] Lueders M, Marques M A L, Floris A, Profeta G, Lathiotakis N N, Franchini C, Sanna A, Continenza A, Massidda S and Gross E K U 2006 Density functional theory for superconductors *Psi-k Newsletter* **76** 54 (Scientific highlight of the month)
[36] QUANTUM ESPRESSO code http://www.quantum-espresso.org/
[37] Marini A SELF code http://www.fisica.uniroma2.it/∼self
[38] Horowitz M, Silvidi A A, Malaker S F and Daunt J G 1952 The specific heat of lead in the temperature range 1 K to 75 K *Phys. Rev.* **88** 1182
[39] Van Der Hoeven B J C Jr and Keesom P H 1965 Specific heat of lead and lead alloys between 0.4 and 4.2 K *Phys. Rev.* A **137** 103
[40] Overhauser A W and Daemen L L 1988 Superconducting gap anisotropy caused by a spin-density wave *Phys. Rev. Lett.* **61** 1885
[41] Richardson C F and Ashcroft N W 1997 High temperature superconductivity in metallic hydrogen: electron–electron enhancements *Phys. Rev. Lett.* **78** 118
[42] Barbee N III, Garía A and Cohen M 1989 First-principles prediction of high-temperature superconductivity in metallic hydrogen *Nature* **340** 369
[43] Zhang L, Niu Y, Li Q, Cui T, Wang Y, Ma Y, He Z and Zou G 2007 *Ab initio* prediction of superconductivity in molecular metallic hydrogen under high pressure *Solid State Commun.* **141** 610
[44] Pickard C J and Needs R J 2007 Structure of phase III of solid hydrogen *Nat. Phys.* **3** 473
[45] Cudazzo P, Profeta G, Sanna A, Floris A, Continenza A, Massidda S and Gross E K U 2008 High-temperature electron–phonon superconductivity in molecular hydrogen under extreme pressure *Phys. Rev. Lett.* **100** 257001
[46] Richardson C F and Ashcroft N W 1997 Effective electron–electron interactions and the theory of superconductivity *Phys. Rev.* B **55** 15130
[47] Cudazzo P *et al* 2009 Superconducting properties of compressed hydrogen from first principles, in preparation
[48] Kong Y, Dolgov O V, Jepsen O and Andersen O K 2001 Electron–phonon interaction in the normal and superconducting states of MgB2 *Phys. Rev.* B **64** 020501
[49] Bohnen K P, Heid R and Renker B 2001 Phonon dispersion and electron–phonon coupling in MgB2 and AlB2 *Phys. Rev. Lett.* **86** 5771
[50] Shukla A, Calandra M, d'Astuto M, Lazzeri M, Mauri F, Bellin C, Krisch M, Karpinski J, Kazakov S M, Jun J, Daghero D and Parlinski K 2003 Phonon dispersion and lifetimes in MgB2 *Phys. Rev. Lett.* **90** 095506
[51] An J M and Pickett W E 2001 Superconductivity of MgB2: covalent bonds driven metallic *Phys. Rev. Lett.* **86** 4366
[52] Brinkman A, Golubov A A, Rogalla H, Dolgov O V, Kortus J, Kong Y, Jepsen O and Andersen O K 2002 Multiband model for tunneling in MgB2 junctions *Phys. Rev.* B **65** 180517
[53] Golubov A A, Brinkman A, Dolgov O V, Kortus J and Jepsen O 2002 Multiband model for penetration depth in MgB2 *Phys. Rev.* B **66** 054524
[54] Dolgov O V, Gonnelli R S, Ummarino G A, Golubov A A, Shulga S V and Kortus J 2003 Extraction of the electron–phonon interaction from tunneling data in the multigap superconductor MgB2 *Phys. Rev.* B **68** 132503